

Can We Determine Electric Fields and Poynting Fluxes from Vector Magnetograms and Doppler Measurements?

G.H. Fisher¹ · B.T. Welsch¹ · W.P. Abbett¹

© Springer ●●●

Abstract The availability of vector-magnetogram sequences with sufficient accuracy and cadence to estimate the temporal derivative of the magnetic field allows us to use Faraday’s law to find an approximate solution for the electric field in the photosphere, using a Poloidal–Toroidal Decomposition (PTD) of the magnetic field and its partial time derivative. Without additional information, however, the electric field found from this technique is under-determined – Faraday’s law provides no information about the electric field that can be derived the gradient of a scalar potential. Here, we show how additional information in the form of line-of-sight Doppler-flow measurements, and motions transverse to the line-of-sight determined with *ad-hoc* methods such as local correlation tracking, can be combined with the PTD solutions to provide much more accurate solutions for the solar electric field, and therefore the Poynting flux of electromagnetic energy in the solar photosphere. Reliable, accurate maps of the Poynting flux are essential for quantitative studies of the buildup of magnetic energy before flares and coronal mass ejections.

Keywords: Flares, Dynamics; Helicity, Magnetic; Magnetic fields, Corona

1. Introduction

The launch of SDO, with its ability to measure the Sun’s vector magnetic field anywhere on the disk with a high temporal cadence, promises to usher in a new era of solar astronomy. This new era of measurement demands new approaches for the analysis and use of this data. We show in this article how the vector magnetic field and Doppler-flow measurements that can now be made with HMI (Scherrer and The HMI Team, 2005) lead to new methods for determining the electric field vector, and the Poynting Flux vector

$$\mathbf{S} = \frac{1}{4\pi} c \mathbf{E} \times \mathbf{B} \quad (1)$$

¹ Space Sciences Laboratory, UC Berkeley, CA, USA
email: fisher@ssl.berkeley.edu, welsch@ssl.berkeley.edu, abbett@ssl.berkeley.edu

at the solar photosphere. The Poynting flux measures the flow of electromagnetic energy at the layers where the magnetic field is determined. Quantitative observational studies of how energy flows into the corona depend on deriving accurate estimates of the Poynting flux.

Most work estimating the Sun’s electric field or Poynting flux either explicitly or implicitly assumes that the electric field is determined by ideal MHD processes, and therefore the problem can be reduced to determining a velocity field associated with the observed magnetic-field evolution. One class of velocity estimation techniques are “Local Correlation Tracking” (LCT) methods, which essentially capture pattern motions of the line-of-sight magnetic field or white-light intensity. This approach was pioneered by November and Simon (1988). Other implementations include the Lockheed–Martin LCT code (Title *et al.*, 1995; Hurlburt *et al.*, 1995), “Balltracking” (Potts, Barrett, and Diver, 2004), and the FLCT code (Fisher and Welsch, 2008). Another class of velocity-estimation methods incorporate solutions of the vertical component of the magnetic induction equation into determinations of the velocity field (Kusano *et al.*, 2002; Welsch *et al.*, 2004; Longcope, 2004; Schuck, 2006, 2008; Chae and Sakurai, 2008). The work we present in this article incorporates solutions of the three-dimensional magnetic induction equation, using the electric field as the fundamental variable, rather than the velocity field.

The temporal evolution of the Sun’s magnetic field is governed by Faraday’s law,

$$\frac{\partial \mathbf{B}}{\partial t} = -\nabla \times c\mathbf{E} . \quad (2)$$

If one can make a map on the photosphere of $\partial \mathbf{B} / \partial t$, can one determine \mathbf{E} by uncurling this equation? Addressing this question was the focus of Fisher *et al.* (2010), in which a poloidal–toroidal decomposition (PTD) of the temporal derivative of the magnetic field was used to invert Faraday’s law to find \mathbf{E} . Fisher *et al.* (2010) found that one could indeed find solutions for \mathbf{E} that solve all three components of Faraday’s law, but the solutions are not unique: the gradient of a scalar function can be added to the PTD solutions for \mathbf{E} without affecting $\nabla \times \mathbf{E}$. Fisher *et al.* (2010) explored two different methods for determining the scalar function using *ad-hoc* and variational methods, both of which enforced the assumption, from ideal MHD, that \mathbf{E} must be normal to \mathbf{B} . Unfortunately, the agreement with a test case from an MHD solution, while better than conventional correlation-tracking methods, was still disappointing. The authors concluded that including additional information from other observed data was one possible approach for improving the electric field inversions.

In this article, we use the same MHD simulation test case used in Welsch *et al.* (2007) and Fisher *et al.* (2010) to show that using Doppler-flow measurements to determine the electric scalar potential, especially in regions where the magnetic field is primarily horizontal, can dramatically improve the inversion for the electric field and the Poynting flux.

In Section 2 we review the PTD formalism that describes how one can derive the purely inductive part of the electric field from measurements that estimate the time derivative of \mathbf{B} , and the technique of Section 3.2 of Fisher *et al.* (2010),

showing how one can derive a potential electric field, which, when added to the inductive part of the electric field, is normal to the magnetic field. This is useful in generating electric-field solutions that are both consistent with Faraday’s law and with ideal MHD, which is generally believed to be a good approximation in the solar photosphere.

Section 3 argues from physical grounds why magnetic-flux emergence may make a large contribution to the part of the electric field attributable to a potential function. Then, starting from this argument, we derive a Poisson equation for an electric-field potential function that is determined primarily from knowledge of the vertical velocity field, as determined from Doppler measurements, and the horizontal magnetic field near polarity inversion lines where the field is nearly horizontal. The electric field from this contribution is then added to that determined from the PTD solutions. We then apply this technique to the MHD simulation test data, to compare the electric field from the simulation with that from PTD alone, and with that from combining PTD with Doppler measurements.

In Section 4, we try a similar approach, but instead of using contributions to the horizontal electric field from Doppler measurements, we use non-inductive contributions to the electric field determined from the FLCT correlation-tracking technique, applicable in regions where the magnetic field is mainly vertical. This technique is essentially the three-dimensional analogue of the ILCT technique described by Welsch *et al.* (2004). We also try combining PTD with contributions from both the Doppler measurements and those from FLCT, and compare with the simulation data.

Our results are summarized in Section 5, along with a discussion of where additional work is needed.

2. Poloidal–Toroidal Decomposition

Here, we present only a brief synopsis of the PTD method of deriving an electric field \mathbf{E} that obeys Faraday’s law. More detail can be found in Section 2 of Fisher *et al.* (2010).

Since the three-dimensional magnetic field vector is a solenoidal quantity, one can express the magnetic field in terms of two scalar functions, \mathcal{B} (the “poloidal” potential) and \mathcal{J} (the “toroidal” potential), as follows:

$$\mathbf{B} = \nabla \times \nabla \times \mathcal{B} \hat{\mathbf{z}} + \nabla \times \mathcal{J} \hat{\mathbf{z}} . \quad (3)$$

Taking the partial time derivative of Equation (3) one finds

$$\dot{\mathbf{B}} = \nabla \times \nabla \times \dot{\mathcal{B}} \hat{\mathbf{z}} + \nabla \times \dot{\mathcal{J}} \hat{\mathbf{z}} . \quad (4)$$

Here, the overdot denotes a partial time derivative. We will now assume a locally Cartesian coordinate system, in which the directions parallel to the photosphere are denoted with a “horizontal” subscript h , and the vertical direction is denoted with subscript z . One can then re-write Equations (3) and (4) in terms of

horizontal and vertical derivatives as

$$\mathbf{B} = \nabla_h \left(\frac{\partial \mathcal{B}}{\partial z} \right) + \nabla_h \times \mathcal{J} \hat{\mathbf{z}} - \nabla_h^2 \mathcal{B} \hat{\mathbf{z}}, \quad (5)$$

and

$$\dot{\mathbf{B}} = \nabla_h \left(\frac{\partial \dot{\mathcal{B}}}{\partial z} \right) + \nabla_h \times \dot{\mathcal{J}} \hat{\mathbf{z}} - \nabla_h^2 \dot{\mathcal{B}} \hat{\mathbf{z}}. \quad (6)$$

One useful property of the poloidal–toroidal decomposition is that the scalar functions $\dot{\mathcal{B}}$, $\dot{\mathcal{J}}$, and $\partial \dot{\mathcal{B}}/\partial z$ can all be determined by knowing the time derivative of the magnetic-field vector in the plane of the photosphere. By examining the z -component of Equation (6), the z -component of the curl of Equation (6), and the horizontal divergence of Equation (6), one can derive the following three two-dimensional Poisson equations for $\dot{\mathcal{B}}$, $\dot{\mathcal{J}}$, and $\partial \dot{\mathcal{B}}/\partial z$:

$$\nabla_h^2 \dot{\mathcal{B}} = -\dot{B}_z, \quad (7)$$

$$\nabla_h^2 \dot{\mathcal{J}} = -(4\pi/c) \dot{J}_z = -\dot{\mathbf{z}} \cdot (\nabla \times \dot{\mathbf{B}}_h), \quad (8)$$

and

$$\nabla_h^2 (\partial \dot{\mathcal{B}}/\partial z) = \nabla_h \cdot \dot{\mathbf{B}}_h. \quad (9)$$

Here, \dot{B}_z and $\dot{\mathbf{B}}_h$ denote the partial time derivatives of the vertical and horizontal components of the magnetic field, respectively. Solving these three Poisson equations provides sufficient information to determine an electric field that satisfies Faraday’s law.

By comparing the form of Equation (2) with Equations (4) and (6) it is clear the following must be true:

$$\nabla \times c\mathbf{E} = -\nabla \times \nabla \times \dot{\mathcal{B}} \hat{\mathbf{z}} - \nabla \times \dot{\mathcal{J}} \hat{\mathbf{z}} \quad (10)$$

$$= -\nabla_h (\partial \dot{\mathcal{B}}/\partial z) - \nabla_h \times \dot{\mathcal{J}} \hat{\mathbf{z}} + \nabla_h^2 \dot{\mathcal{B}} \hat{\mathbf{z}}. \quad (11)$$

Uncurling Equation (10) yields this expression for the electric field \mathbf{E} :

$$c\mathbf{E} = -\nabla \times \dot{\mathcal{B}} \hat{\mathbf{z}} - \dot{\mathcal{J}} \hat{\mathbf{z}} - c\nabla\psi \equiv c\mathbf{E}^I - c\nabla\psi. \quad (12)$$

Here, $-\nabla\psi$ is the contribution to the electric field from a scalar potential, for which solutions to Faraday’s law reveal no information. The solution for \mathbf{E} without the contribution from $-\nabla\psi$, \mathbf{E}^I , is the purely inductive solution determined from the PTD method. Within this article, this solution will be referred to simply as the PTD solution or the PTD electric field. Note that the PTD solution is not unique. While solutions for $\partial \dot{\mathcal{B}}/\partial z$ are necessary to ensure that Faraday’s law is obeyed, the PTD solution for the electric field itself depends only on $\dot{\mathcal{B}}$ and $\dot{\mathcal{J}}$. This means that the PTD electric field is the same for distributions of \dot{B}_z and $\dot{\mathbf{B}}_h$ which have differing values of $\nabla_h \cdot \dot{\mathbf{B}}_h$, but the same values of $(\nabla_h \times \dot{\mathbf{B}}_h) \cdot \hat{\mathbf{z}}$ and \dot{B}_z . Thus the PTD solutions for \mathbf{E}^I are under-determined.

Fisher *et al.* (2010) described two techniques for deriving an electric-field contribution from a scalar potential, in an effort to resolve the under-determined nature of the PTD solutions. The first technique, described in Section 3.2 of that article, presents an *ad-hoc* iterative method for deriving a scalar potential electric field which, when added to the PTD solution, results in an electric field that is normal to \mathbf{B} , and hence consistent with ideal MHD. The second technique, based on a variational method, finds a scalar potential electric field that, when added to the PTD solution, minimizes the area integral of $|\mathbf{E}|^2$ or $|\mathbf{v}|^2$. When compared to the original electric field from the simulation test case, the iterative method applied to the PTD solutions showed a qualitative consistency, but not detailed agreement with the simulation electric field, while the electric field computed with the variational technique showed poor agreement. Fisher *et al.* (2010) concluded that significant improvement in the agreement of the inverted electric field with the real electric field requires additional observational information beyond the temporal evolution of \mathbf{B} .

3. The Importance of Doppler Flow Measurements to the Electric Field

We argue here that when flux emergence occurs, much of the missing information about non-inductive contributions to the electric field is contained in Doppler flow information (see also Ravindra, Longcope, and Abbett, 2008 and Schuck *et al.*, 2010), particularly near polarity inversion lines (PILs), where the horizontal magnetic field is much stronger than the vertical field. We illustrate this point with a simple thought-experiment, shown schematically in Figure 1. Consider the emergence of new magnetic flux in an idealized bipolar-flux system, where the PIL maintains its orientation as flux continuously emerges from below the photosphere. Imagine that vector magnetogram and Doppler observations are taken from a vantage point normal to the solar surface. Let us focus attention on what is happening near the center of the PIL. Suppose the magnetic field there remains time-invariant as flux continues to emerge, so the time derivative of the magnetic field there is zero, implying that Faraday's law cannot be used to infer the physics of the emerging flux. Yet the electric field at this location should be very large, driven by the upward motion of the plasma carrying the strong, horizontal field. In this case, magnetic-flux emergence will have a strong inductive signature at the edges of the idealized active region, where the vertical magnetic field is changing rapidly, but not near the center of the PIL. Thus, it seems plausible that the electric field near PILs in more realistic emerging-flux configurations will have a significant non-inductive component.

Starting from this perspective, we have explored enhancements to the PTD method that use Doppler flow information to more tightly constrain the PTD electric field solutions, with the additional assumption that the photospheric electric field is primarily governed by ideal MHD processes. Directly above PILs, the vertical velocity and the observed horizontal component of the magnetic field unambiguously determine the horizontal electric field:

$$c\mathbf{E}_h^D = -v_z \hat{\mathbf{z}} \times \mathbf{B}_h, \quad (13)$$

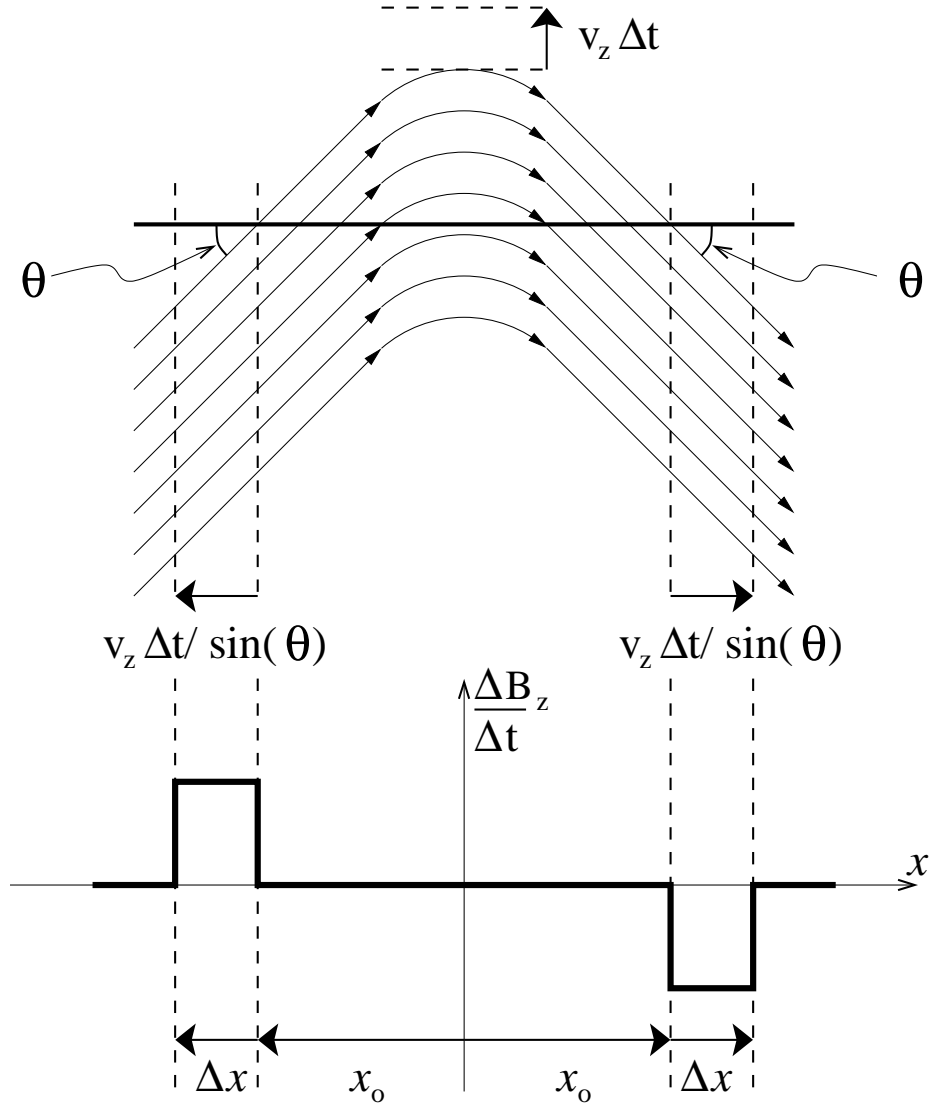


Figure 1. Schematic illustration of the emergence of new flux over a time interval Δt , viewed in a vertical plane normal to the polarity inversion line (PIL) in an idealized bipolar flux system. The emerging flux is rising at a speed v_z , which could be inferred by the Doppler shift measured by an observer viewing the PIL from above. The width of the bipolar flux system (the distance from the outer edge of one pole to the outer edge of the other pole) at the beginning of Δt is $2x_0$. Notice that the change in B_z at the outer edges of the emerging flux region is large, while the change in B_z at the PIL itself — where the flux is actually emerging — is zero (see text).

where we assume that $|B_z|/|B_h|$ is small. If we can use line-of-sight Doppler velocity measurements to estimate v_z , we add a powerful constraint to the PTD solution for the electric field. Of course, we would like to use the Doppler information away from PILs as well, but are hindered by two complications: *i*) flows parallel to the magnetic field will not affect the electric field at all, but may contribute to the observed Doppler velocity signal, and *ii*) when the vertical component of the magnetic field $[B_z]$ becomes significant compared to the horizontal field $[B_h]$, there is an additional contribution to the horizontal electric field from flow parallel to the surface, which is not accounted for.

We now develop a formal solution for a non-inductive contribution to the electric field that includes information from Doppler-shift measurements, and apply it to a test case with a known electric field. First, from the pair of synthetic vector magnetograms taken from the ANMHD simulation test case described in Welsch *et al.* (2007) and Section 3.1 of Fisher *et al.* (2010), we use the PTD method to find an electric-field solution, neglecting any contribution from a scalar electric-field potential function. We use the numerical techniques and boundary conditions described in Section 3.1 of Fisher *et al.* (2010). Second, we compute a candidate horizontal electric field from vertical velocities taken from the simulation as synthetic Doppler-flow measurements, and horizontal magnetic fields from the synthetic vector magnetograms, from Equation (13) above. This electric field is then multiplied by a “confidence function”, which is near unity at PILs, but decreases to zero when $|B_z/B_h|$ is no longer small. This reflects our lack of confidence in the accuracy of this horizontal Doppler electric field in those locations, for the reasons described earlier. The specific form for the confidence function is probably not important. Here, we assume the confidence function w is given by

$$w = \exp[-(|B_z|/|B_h|)^2/\sigma^2] , \quad (14)$$

where σ is a free parameter that can be adjusted, and in the specific cases shown in this article was set somewhat arbitrarily to 0.6. We define the “modulated” electric field within the plane of the magnetogram as

$$\mathbf{E}_h^M = w\mathbf{E}_h^D \quad (15)$$

Third, we take the divergence of this modulated horizontal electric field \mathbf{E}_h^M , and find the electric-potential function that can best represent it by setting

$$c\mathbf{E}^X = -\nabla_h\chi , \quad (16)$$

where χ solves the Poisson equation

$$\nabla_h^2\chi = -\nabla_h \cdot c\mathbf{E}_h^M . \quad (17)$$

Because the synthetic vector magnetograms and Doppler flows taken from the MHD simulation use periodic boundary conditions, we use FFT techniques to solve Equation (17). Adding this contribution onto the PTD solutions means that information about the electric field at PILs has been incorporated, while

also maintaining consistency with Faraday’s Law, since \mathbf{E}^χ has no curl. Since we generally expect ideal MHD to be a good approximation for conditions in the solar photosphere, we then remove the components of \mathbf{E} parallel to \mathbf{B} by adding the electric field from a second potential function ψ , using the iterative technique described in Section 3.2 of Fisher *et al.* (2010):

$$c\mathbf{E}^{\text{tot}} = c\mathbf{E}^I + c\mathbf{E}^\chi - \nabla\psi , \quad (18)$$

where $\nabla\psi \cdot \mathbf{B} = (c\mathbf{E}^I + c\mathbf{E}^\chi) \cdot \mathbf{B}$.

The resulting solutions for \mathbf{E} are shown in the third row of Figure 2, with a scatterplot comparison of S_z of the PTD method and the PTD plus Doppler information with the actual simulation electric fields shown in the top two panels of Figure 3. These portions of the figures show that the recovery of the electric-field components and the Poynting flux is dramatically better than PTD alone.

4. How Important are Horizontal, Non-Inductive Flows?

In the previous section, we considered the role of Doppler-flow measurements in determining non-inductive contributions to the horizontal electric field, and found that combining this information with the PTD solutions for Faraday’s law results in a dramatic improvement in the recovery of the electric field. However, this treatment neglects possible contributions to the horizontal electric field away from PILs where a cross product of horizontal velocity with vertical magnetic field could also contribute to the horizontal electric field. Contributions to the horizontal electric field that solve the induction equation have already been incorporated by the PTD solutions, but as with vertical velocities, there could be a sub-space of horizontal flows that do not contribute to Faraday’s law.

To evaluate this effect, we estimate horizontal velocities using the FLCT local-correlation tracking (LCT) code (see Fisher and Welsch, 2008), available from http://solarmuri.ssl.berkeley.edu/~fisher/public/software/FLCT/C_VERSIONS/ using images of the vertical component of the magnetic field. Velocities were not computed for pixels with a vertical magnetic field strength below 370G (see discussion in Welsch *et al.*, 2007), with the windowing parameter σ set to five pixels. The low-pass filtering option was not invoked. The result is a map of the apparent horizontal-velocity field [$\mathbf{U}_h \equiv U_x\hat{\mathbf{x}} + U_y\hat{\mathbf{y}}$] computed at the strong vertical magnetic-field locations, and with velocities at all other locations set to zero. A candidate horizontal electric field is estimated by setting

$$c\mathbf{E}_h^{\text{LCT}} = -\mathbf{U}_h \times \hat{\mathbf{z}}B_z . \quad (19)$$

To consider only non-inductive contributions from \mathbf{U}_h , we perform the same general operation as in the previous section, namely to multiply $\mathbf{E}_h^{\text{LCT}}$ by a confidence function, and then eliminate the inductive part of the electric field. Here, the confidence function will be the complement of the confidence function used for the Doppler case, since the LCT estimates are nearly useless near PILs, where the Doppler results should be reliable, while the LCT results should be best when

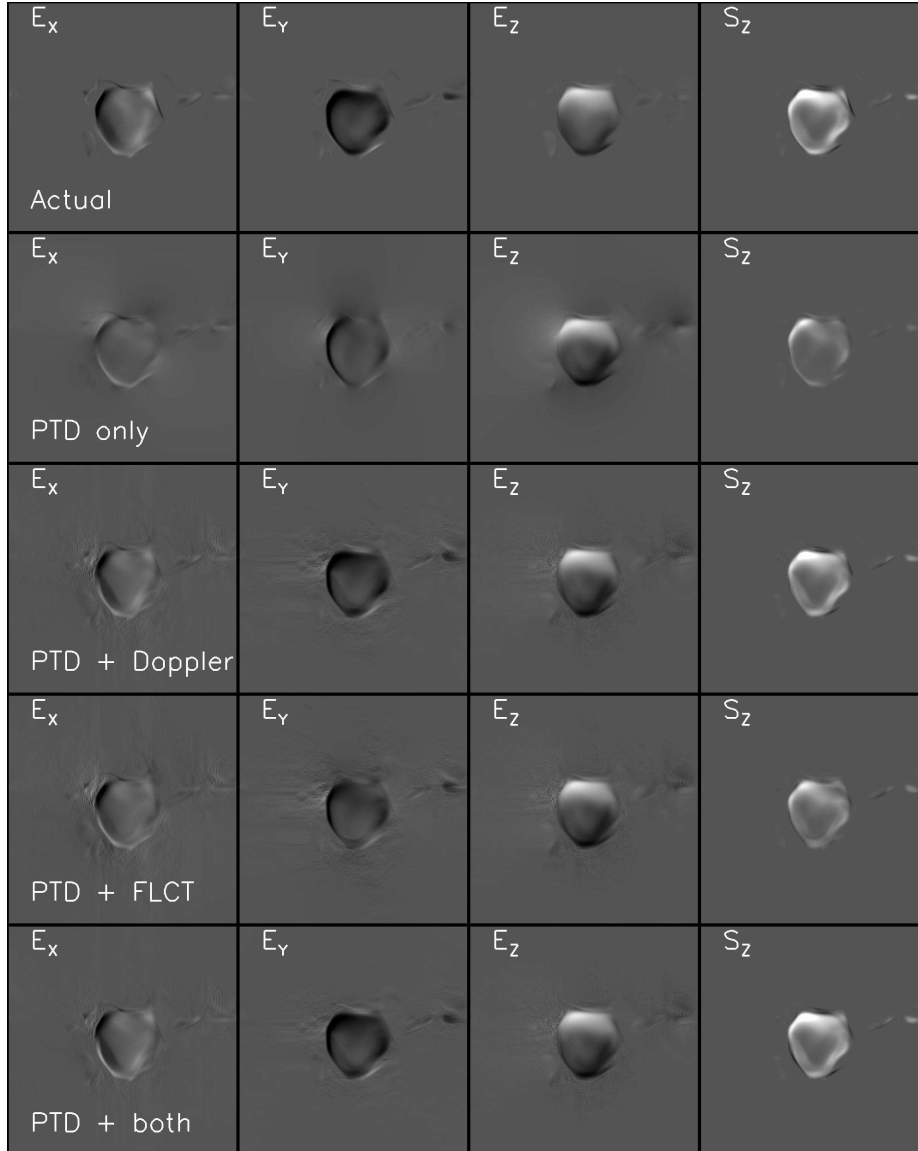


Figure 2. Top row: The three components of the electric field and the vertical Poynting flux from the MHD reference simulation of emerging magnetic flux in a turbulent convection zone. Second row: The inductive components of \mathbf{E} and S_z determined using the PTD method. Third row: \mathbf{E} and S_z derived by incorporating Doppler flows around PILs into the PTD solutions. Note the dramatic improvement in the estimate of S_z . Fourth row: \mathbf{E} and S_z derived by incorporating only non-inductive FLCT derived flows into the PTD solutions. Note the poorer recovery of E_x , E_y , and S_z relative to the case that included only Doppler flows. Fifth row: \mathbf{E} and S_z derived by including both Doppler flows and non-inductive FLCT flows into the PTD solutions. Note the good recovery of E_x , E_y , and S_z , and the reduction in artifacts in the low-field regions for E_y (best viewed in the electronic version of the article).

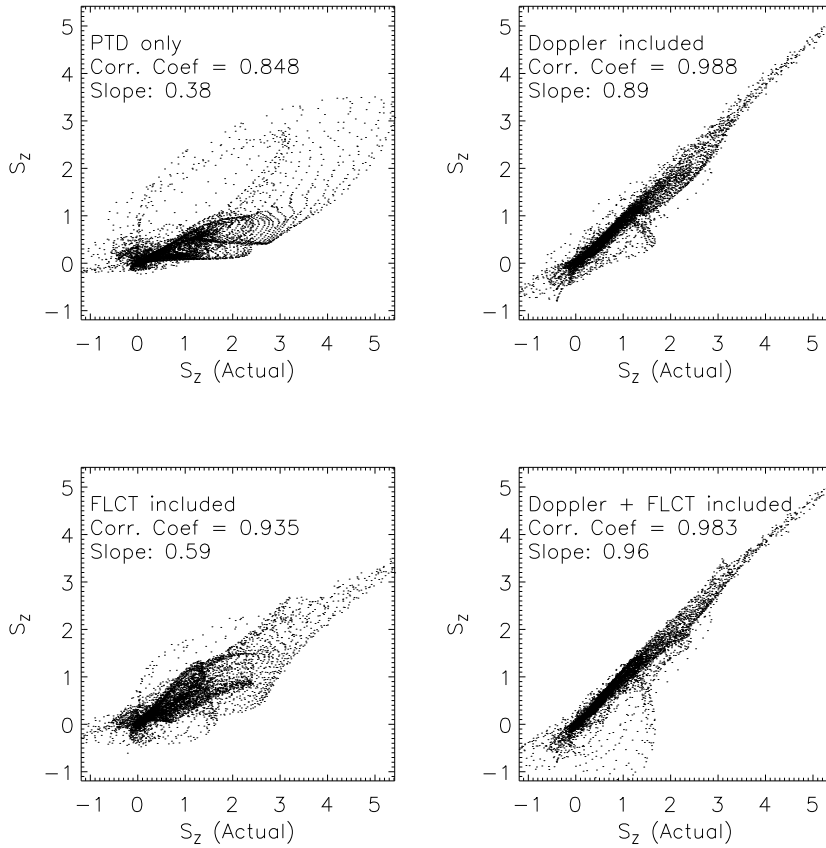


Figure 3. Upper left: A comparison of the vertical component of the Poynting flux derived from the PTD method alone with the actual Poynting flux of the MHD reference simulation. Upper right: A comparison between the simulated results and the improved technique that incorporates information about the vertical flow field around PILs into the PTD solutions. Lower left: Comparison of the vertical Poynting flux when non-inductive FLCT-derived flows are incorporated into the PTD solutions. Lower right: Comparison of the vertical Poynting flux when both Doppler flow information and non-inductive FLCT-derived flows are incorporated into the PTD solutions. Each scatterplot also shows the computed linear correlation coefficient, as well as the slope of the fit derived with IDL’s LADFIT function. Poynting flux units are in [$10^5 \text{ G}^2 \text{ km s}^{-1}$]

the magnetic field is mostly vertical (and where the Doppler measurements are useless).

We define $c\mathbf{E}^\zeta = -\nabla_h \zeta$, and assume that

$$\nabla_h^2 \zeta = -\nabla_h \cdot (1-w)c\mathbf{E}_h^{\text{LCT}} \quad (20)$$

Once this equation has been solved and \mathbf{E}^ζ has been computed, it can be added to the PTD solutions for \mathbf{E}^I , and as in the previous section, a second potential solution can be found that eliminates components of \mathbf{E} parallel to

B. Note that combining the PTD solutions with \mathbf{E}^{ζ} in this way is like the approach used in the ILCT technique described by Welsch *et al.* (2004), except that solutions of a single component of the induction equation are replaced by solutions to all three components of the induction equation.

The resulting electric field and Poynting flux can be compared to the actual case, the un-altered PTD case, and the case where only the Doppler information is used. The electric field and Poynting flux results are shown as the fourth row of panels in Figure 2 and a scatterplot of the Poynting flux values with the actual values is shown in the lower left panel of Figure 3. While the overall performance of the FLCT case is better than that of PTD alone, it is not significantly better than simply applying the iterative method directly to the PTD results as was described in Section 3.2 of Fisher *et al.* (2010). It is definitely not as good as the performance we show from the Doppler-only case. We conclude that most of the useful information about the non-inductive electric field, at least for this particular simulation of strong flux emergence, is contained within the Doppler flow information.

Does the LCT information, when added to the Doppler-flow information, significantly improve the resulting estimate for the electric field? To answer this question, we have added both the LCT and Doppler electric-field information to the PTD solutions, and again found a potential function to eliminate components of \mathbf{E} parallel to \mathbf{B} . The resulting electric field and Poynting-flux maps are shown in the fifth row of panels in Figure 2, and a scatterplot of the vertical Poynting flux is shown in the lower-right panel of Figure 3.

The linear correlation coefficient in the Poynting-flux scatterplot is not significantly improved by adding the LCT results to the Doppler results, but the slope of the fit (determined by using IDL's LADFIT function) is somewhat better. Further, examining the maps of E_x and E_y show a reduction in artifacts in the behavior of the recovered electric-field components, compared to the Doppler and LCT cases. We conclude that at least for this simulation, which exhibited strong flux emergence, most of the additional useful information beyond solutions to Faraday's law is contained within the Doppler velocity measurements, with some additional improvement when non-inductive LCT-derived electric fields are added.

Finally, we wish to add a comment about solutions to the PTD equations themselves. The PTD solutions used in this article did not use FFT solutions for $\dot{\mathbf{B}}$ and $\dot{\mathcal{J}}$, even though the simulations are periodic, but instead used Neumann boundary conditions for $\dot{\mathbf{B}}$ for the reasons described in Section 2.2 of Fisher *et al.* (2010). For the current study, we compared the results of using FFT solutions of the PTD equations with those shown in the figures in this article, and found noticeable degradations in the fits of the model Poynting fluxes to the actual model values. If one is interested in the most accurate reconstruction of the vertical Poynting flux, we recommend not using FFT solutions of the PTD equations.

5. Discussion and Conclusions

We have reviewed how the PTD solutions of Faraday’s law for \mathbf{E} can be found using temporal sequences of vector magnetograms that can be obtained with the HMI instrument on NASA’s SDO mission. We discussed why these solutions are under-determined, and the importance of determining the contributions to the electric field that can be derived from a scalar potential.

We demonstrate, using simulation data where the true electric field is known, that knowledge of the vertical-velocity field (obtainable by Doppler measurements) can provide important information about the electric field. When this information is combined with the PTD solutions of Faraday’s law, dramatically more accurate recovery of the true electric field is possible. We find that additional information about flows from local correlation-tracking methods can also be combined with the PTD solutions, but the additional information is significantly less important than that from the Doppler measurements. We are able to quantitatively reconstruct the electromagnetic Poynting flux in the simulations by using our combination of the PTD solutions and those from Doppler measurements.

This “proof-of-concept” demonstration argues strongly for the development of electric-field and Poynting-flux tools to be used routinely in the analysis of HMI vector magnetic-field measurements. Routinely available Poynting-flux maps will be useful for scientific studies of flare-energy buildup, understanding the flow of magnetic energy in the solar atmosphere prior to CME initiation, and will aid in understanding the flow of energy that heats the corona. Further, the PTD formalism for the magnetic field itself (Equation (5)) allows for a straight-forward decomposition of the Poynting flux into changes in the potential-field energy, and the flux of free magnetic energy (see Welsch, 2006 and the end of Section 2.1 of Fisher *et al.*, 2010). The flux of free magnetic energy is especially important in determining how energy builds up in flare-productive active regions.

To find solutions for \mathbf{E} and the Poynting flux \mathbf{S} using the PTD formalism plus Doppler measurements requires only the solution of three two-dimensional Poisson equations. While real vector-magnetogram patches will not have periodic boundary conditions (as were employed in this article), straightforward numerical techniques exist to solve these equations routinely. Preliminary investigations also indicate that generalizing the PTD solutions and Doppler measurements to cases of non-normal viewing angle will be straightforward. In our opinion, the major obstacle that remains before such solutions can be routinely applied to the HMI data, is a detailed understanding of how measurement errors and disambiguation errors in the vector magnetograms will affect the solutions, and how the effects of these errors are best ameliorated.

Acknowledgements This research was funded by the NASA Heliophysics Theory Program (grant NNX08AI56G), the NASA Living-With-a-Star TR&T Program (grant NNX08AQ30G), by the NSF SHINE program (grants ATM0551084 and ATM0752597), and support from NSF’s AGS Program (grant ATM0641303) for our participation in the University of Michigan’s CCHM Project. The authors are grateful to US taxpayers for providing the funds necessary to perform this work. The authors wish to acknowledge Dick Canfield for his pioneering work in

the use of vector magnetograms in solar physics. The inspiration for the work described here can be traced to a Solar MURI workshop held at UC Berkeley in 2002, in which Dick Canfield played a major role in defining long-term research goals for the use of vector magnetograms in quantitative models of the Sun's atmosphere.

References

- Chae, J., Sakurai, T.: 2008, A Test of Three Optical Flow Techniques-LCT, DAVE, and NAVE. *Astrophys. J.* **689**, 593–612. doi:10.1086/592761.
- Fisher, G.H., Welsch, B.T.: 2008, FLCT: A Fast, Efficient Method for Performing Local Correlation Tracking. In: Howe, R., Komm, R.W., Balasubramaniam, K.S., Petrie, G.J.D. (eds.) *Subsurface and Atmospheric Influences on Solar Activity*, **CS-383**, Astronom. Soc. Pacific, San Francisco, 373–380 (also arXiv:0712.4289).
- Fisher, G.H., Welsch, B.T., Abbett, W.P., Bercik, D.J.: 2010, Estimating Electric Fields from Vector Magnetogram Sequences. *Astrophys. J.* **715**, 242–259. doi:10.1088/0004-637X/715/1/242.
- Hurlburt, N.E., Schrijver, C.J., Shine, R.A., Title, A.M.: 1995, Simulated MDI Observations of Convection. In: Hoeksema, J.T., Domingo, V., Fleck, B., Battrick, B. (eds.) *Helioseismology SP-376*, ESA, Noordwijk, 239.
- Kusano, K., Maeshiro, T., Yokoyama, T., Sakurai, T.: 2002, Measurement of magnetic helicity injection and free energy loading into the solar corona. *Astrophys. J.* **577**, 501–512.
- Longcope, D.W.: 2004, Inferring a photospheric velocity field from a sequence of vector magnetograms: the minimum energy fit. *Astrophys. J.* **612**, 1181–1192.
- November, L.J., Simon, G.W.: 1988, Precise proper-motion measurement of solar granulation. *Astrophys. J.* **333**, 427–442.
- Potts, H.E., Barrett, R.K., Diver, D.A.: 2004, Balltracking: An highly efficient method for tracking flow fields. *Astron. Astrophys.* **424**, 253–262. doi:10.1051/0004-6361:20035891.
- Ravindra, B., Longcope, D.W., Abbett, W.P.: 2008, Inferring Photospheric Velocity Fields Using a Combination of Minimum Energy Fit, Local Correlation Tracking, and Doppler Velocity. *Astrophys. J.* **677**, 751–768. doi:10.1086/528363.
- Scherrer, P.H., The HMI Team: 2005, The helioseismic and magnetic imager for the solar dynamics observatory. *AGU Spring Meeting Abstracts*, 43–05.
- Schuck, P.W.: 2006, Tracking Magnetic Footpoints with the Magnetic Induction Equation. *Astrophys. J.* **646**, 1358–1391. doi:10.1086/505015.
- Schuck, P.W.: 2008, Tracking Vector Magnetograms with the Magnetic Induction Equation. *Astrophys. J.* **683**, 1134–1152. doi:10.1086/589434.
- Schuck, P.W., Sun, X., Muglach, K., Hoeksema, J.T.: 2010, Tracking Vector Magnetograms from the Solar Dynamics Observatory. *AGU Fall Meeting Abstracts*, A7.
- Title, A.M., Hurlburt, N.E., Schrijver, C.J., Shine, R.A., Tarbell, T.: 1995, Observations of Convection. In: Hoeksema, J.T., Domingo, V., Fleck, B., Battrick, B. (eds.) *Helioseismology SP-376*, ESA, Noordwijk, 113.
- Welsch, B.T.: 2006, Magnetic Flux Cancellation and Coronal Magnetic Energy. *Astrophys. J.* **638**, 1101–1109. doi:10.1086/498638.
- Welsch, B.T., Fisher, G.H., Abbett, W.P., Regnier, S.: 2004, ILCT: Recovering Photospheric Velocities from Magnetograms by Combining the Induction Equation with Local Correlation Tracking. *Astrophys. J.* **610**, 1148–1156. doi:10.1086/421767.
- Welsch, B.T., Abbett, W.P., DeRosa, M.L., Fisher, G.H., Georgoulis, K., Kusano, M.K., Longcope, D.W., Ravindra, B., Schuck, P.W.: 2007, Tests and comparisons of velocity inversion techniques. *Astrophys. J.* **670**, 1434–1452.

